



A novel modification of decouple scaled boundary finite element method in fracture mechanics problems

M. Yazdani*

¹Department of Civil Engineering, Faculty of Engineering, Arak University, Arak, Iran

Article info:

Received: 27/08/2016

Accepted: 25/12/2017

Online: 10/03/2018

Keywords:

Decoupled scaled boundary finite element method (DSBFEM), Linear elastic fracture mechanics (LEFM), Fracture parameters, Lagrange polynomials, Gauss-Lobatto-Legendre integration,

Abstract

In fracture mechanics and failure analysis, cracked media energy and consequently stress intensity factors (SIFs) play a crucial and significant role. Based on linear elastic fracture mechanics (LEFM), the SIFs and energy of cracked media may be estimated. This study presents the novel modification of decoupled scaled boundary finite element method (DSBFEM) to model cracked media. In this method, only the boundaries of problems are discretized using specific higher-order sub-parametric elements and higher-order Lagrange polynomials as mapping functions. Implementing the weighted residual method and using Gauss-Lobatto-Legendre numerical integration yield diagonal Euler's differential equations. The chief modifications among the research conducted and the previous studies concerning DSBFEM is that here in, generation of geometry process of the functional interpolation, integration of the diverse is chosen, and by current technic, the difficulty of the DSBFEM is decreased. Therefore, when the local coordinates origin is located at the crack tip, the geometry of crack problems are implemented directly without further processing. Validity and accuracy of the proposed method are fully illustrated through three benchmark problems, whose results agree very well with those of other numerical and/or analytical solutions existing in the literature.

1. Introduction

The existence of crack and notch may cause remarkable concerns in the failure analysis of solids and structures. In order to analyze this type of engineering subjects, the stress intensity factors (SIFs) are used to survey singularity at the crack tips. Since the majority of these problems do not have closed-form solutions [1, 2], numerical methods are usual approaches to deal with fracture mechanics problems.

According to linear elastic fracture mechanics (LEFM), various classes of numerical methods such as finite element method (FEM), boundary element method (BEM), extended finite element method (XFEM), meshless methods, fractal-like finite element method (FFEM), scaled boundary finite element method (SBFEM), and hybrid methods have been extensively developed to compute the SIFs of crack tips for simulation of crack problems in brittle or quasi-brittle materials.

*Corresponding author
email address: m-yazdani@araku.ac.ir

The FEM is employed frequently in the analysis of fracture mechanics problems because of its flexibility [3–8]. Some disadvantages of FEM lead to the development of the other numerical methods. For example, due to the difficulties of remeshing techniques to predict crack propagation, the XFEM is elaborated [9–12]. Similarly, since very fine crack tip meshes require high computational efforts in the FEM, the BEM is used in the fracture analysis, as an alternative method. Although the BEM does not require domain discretization but the boundaries, the computational costs are dramatically reduced. However, the BEM needs a fundamental solution for the governing differential equations as well as relatively advanced mathematical techniques to calculate the singular integrals (see for example [13–17] among others). Also, FEM is not the perfect numerical method to be used in fracture mechanics issues as stress singularity at the crack tips is not modeled precisely. Thus, the strain energy approach is recently developed by Treifi and Oyadiji [18, 19], in which stresses at the notch tip vicinity are evaluated by means of the distributed dislocation technics. Larrosa *et al.* [20] presented a methodology to evaluate the strain energy density and notch SIF, rapidly. The meshless methods have become another attractive approach for fracture mechanics problems. These methods do not require any discretization of the problem domain, and therefore the approximate solution of the problem is gained using a set of dispersed nodes. One of the attractions of the meshless methods may be devoted to their flexibility in dealing with discontinuities (such as cracks) [21–26]. The FFEM was first developed to calculate the SIFs for cracked domains [27]. In this method, the global interpolation functions, which are the analytical solutions of the displacement patterns near the crack tip, are used. Although the analytical solutions do not satisfy the boundary conditions in general, the FFEM considers the boundary conditions by master nodes. The SBFEM combines the advantages of both the FEM and BEM with its own unique features and has shown its efficiency and accuracy for determining the SIFs (e.g., [28–31]). On the other hand, the

hybrid methods as popular methods by combining the advantages of different numerical methods are widely used to compute SIFs [32–36].

A modification of the SBFEM, so-called decoupled scaled boundary finite element method (DSBFEM), has been developed by Khaji and Khodakarami for potential problems [37], elastostatic problems [38], elastodynamic problems [39], and fracture mechanics problems [40–42]. In this study, the efficiency and reduced complexity of the DSBFEM, which have been proposed in [37–42], has improved for fracture mechanics issues, where the Lagrange polynomials is used as mapping functions instead of Chebyshev polynomials, and also Gauss-Lobatto-Legendre (GLL) quadrature is employed instead of Clenshaw-Curtis integration technique in order to calculate the coefficient matrices. By the way, with implementing this technique, the governing equations for each node are independent of the other nodes, and this will reduce the computational costs because the evaluation of matrices and vectors and obtaining the solution procedure is easier while one employs Lagrange polynomial and GLL quadrature [43]. Furthermore, the fracture's parameters at the crack tip based on the LEFM are extracted based on the new modification. Finally, some benchmark problems are modeled using the modified DSBFEM to illustrate validity and accuracy of the achieved outcomes.

2. Fundamentals of the semi-analytical method

As this paper demonstrates, a novel modification of DSBFEM for the analysis of crack's issues; the main concepts of the DSBFEM are given here. In other words, the emphasis is primary devoted to those important aspects of the method which are subjected to remarkable modifications in comparison with the previous works of the authors [37–42]. For more details on the formulation of the DSBFEM, the readers are referred to Ref. [38]. In the DSBFEM, the so-called local coordinates origin (LCO) is selected at a point, from which the entire domain boundary can be detected. For

the bounded domains, as a major category of solid mechanics problems, the LCO may be selected on the boundary or inside the domain Ω . Furthermore, only the boundaries that do not pass through the LCO need to be discretized, while other rest boundaries passing through the LCO are not required to be discretized (e.g., Γ_1 and Γ_6 in Fig. 1(a)).

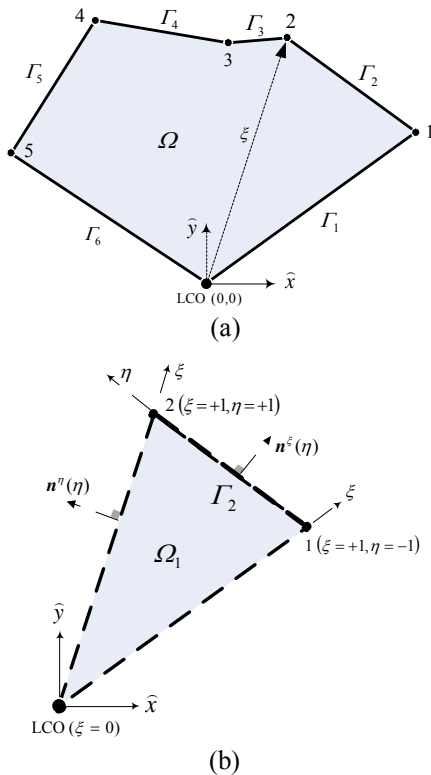


Fig. 1. Modeling of 2D bounded domain in (a) global and (b) local coordinates systems.

As may be seen from Fig. 1(b), one-dimensional (1D) elements are used to discretize the boundaries which do not pass through the LCO, at which $\hat{x} = \hat{y} = 0$. In Fig. 1(b), only the first and the last nodes of the 1D element are displayed. Using Chebyshev polynomials as mapping functions, the geometry of the problem may be transformed from global Cartesian coordinate (\hat{x}, \hat{y}) to local dimensionless coordinates (ξ, η) . The radial coordinate $\xi \in [0, +1]$ varies between the LCO and the boundaries. The tangential coordinate

$\eta \in [-1, +1]$ are defined on boundaries that do not pass through the LCO.

Location of the nodes of the 1D element on the boundaries is measured by x and y in the global Cartesian coordinates. If the global coordinates of the i th node of each element on the boundaries are indicated by x_i and y_i , the element may be defined in terms of a set of n_η mapping functions $\varphi_i(\eta)$, for which $i = 1, 2, \dots, n_\eta + 1$. In other words, the geometry of the element is interpolated using the mapping functions $\boldsymbol{\varphi}(\eta)$ in the local coordinates as:

$$\mathbf{x}(\eta) = \boldsymbol{\varphi}(\eta)\mathbf{x} \tag{1}$$

or

$$x(\eta) = \sum_{i=1}^{n_\eta+1} \varphi_i(\eta)x_i, y(\eta) = \sum_{i=1}^{n_\eta+1} \varphi_i(\eta)y_i \tag{2}$$

where

$$\mathbf{x}(\eta) = \begin{Bmatrix} x(\eta) \\ y(\eta) \end{Bmatrix} \tag{3}$$

Also

$$\mathbf{x} = \{x_1, y_1, x_2, y_2, \dots, x_{n_\eta+1}, y_{n_\eta+1}\}^T \tag{4}$$

implies nodal points' coordinates of an element in the local Cartesian coordinates, and

$$\boldsymbol{\varphi}(\eta) = [\varphi_1(\eta)\mathbf{I}, \varphi_2(\eta)\mathbf{I}, \dots, \varphi_{n_\eta+1}(\eta)\mathbf{I}] \tag{5}$$

in which \mathbf{I} denotes an 2×2 identity matrix. In this method, any given point inside the domain with (\hat{x}, \hat{y}) coordinates is related to the corresponding point on the elements of boundaries by the following relations:

$$\hat{x}(\xi, \eta) = \xi x(\eta) = \xi \sum_{i=1}^{n_\eta+1} \varphi_i(\eta)x_i \tag{6}$$

$$\widehat{y}(\xi, \eta) = \xi y(\eta) = \xi \sum_{i=1}^{n_\eta+1} \varphi_i(\eta) y_i \quad (7)$$

In the DSBFEM, the relation between a differential element of area $d\widehat{x} d\widehat{y}$ (in the global coordinates) and $d\xi d\eta$ (in the local coordinates) is introduced by:

$$d\Omega = d\widehat{x} d\widehat{y} = |\widehat{J}(\xi, \eta)| d\xi d\eta = \xi |J(\eta)| d\xi d\eta \quad (8)$$

where $\widehat{J}(\xi, \eta)$ denotes the Jacobian matrix of transformation as:

$$\widehat{J}(\xi, \eta) = \begin{bmatrix} \widehat{x}_{,\xi}(\xi, \eta) & \widehat{y}_{,\xi}(\xi, \eta) \\ \widehat{x}_{,\eta}(\xi, \eta) & \widehat{y}_{,\eta}(\xi, \eta) \end{bmatrix} \quad (9)$$

Furthermore, the Jacobian matrix on the boundary is shown to be written as:

$$J(\eta) = \begin{bmatrix} x(\eta) & y(\eta) \\ x_{,\eta}(\eta) & y_{,\eta}(\eta) \end{bmatrix} \quad (10)$$

By introducing the differential operator L , a virtual vector $s = \{s_{\widehat{x}}, s_{\widehat{y}}\}^T$ in the global coordinates system is related to its spatial derivatives by:

$$\begin{Bmatrix} s_{,\widehat{x}} \\ s_{,\widehat{y}} \\ s_{,\widehat{x}} + s_{,\widehat{y}} \end{Bmatrix} = L \begin{Bmatrix} s_{\widehat{x}} \\ s_{\widehat{y}} \end{Bmatrix} \quad (11)$$

in which

$$L = \begin{bmatrix} \partial/\partial\widehat{x} & 0 \\ 0 & \partial/\partial\widehat{y} \\ \partial/\partial\widehat{y} & \partial/\partial\widehat{x} \end{bmatrix} \quad (12)$$

It may be shown that the differential operator L is rewritten as:

$$L = \mathbf{b}^1(\eta) \frac{\partial}{\partial\xi} + \frac{1}{\xi} \mathbf{b}^2(\eta) \frac{\partial}{\partial\eta} \quad (13)$$

where

$$\mathbf{b}^1(\eta) = \frac{1}{|J(\eta)|} \begin{bmatrix} y_{,\eta}(\eta) & 0 \\ 0 & -x_{,\eta}(\eta) \\ -x_{,\eta}(\eta) & y_{,\eta}(\eta) \end{bmatrix} \quad (14)$$

$$\mathbf{b}^2(\eta) = \frac{1}{|J(\eta)|} \begin{bmatrix} -y(\eta) & 0 \\ 0 & x(\eta) \\ x(\eta) & -y(\eta) \end{bmatrix} \quad (15)$$

To compute the surface traction, the unit normal vector \mathbf{n} on the boundary may be defined as:

$$\mathbf{n} = \frac{1}{|\nabla\mathbf{x}(\eta)|} \nabla\mathbf{x}(\eta) \quad (16)$$

By substituting Eqs. (1 and 3) into Eq. (16), the unit normal vectors $\mathbf{n}^\xi(\eta)$ and $\mathbf{n}^\eta(\eta)$ are calculated as given by (see Fig. 1(b)):

$$\mathbf{n}^\xi(\eta) = \frac{1}{\left| \begin{Bmatrix} y_{,\eta}(\eta) \\ -x_{,\eta}(\eta) \end{Bmatrix} \right|} \begin{bmatrix} y_{,\eta}(\eta) & 0 \\ 0 & -x_{,\eta}(\eta) \\ -x_{,\eta}(\eta) & y_{,\eta}(\eta) \end{bmatrix} \quad (17)$$

$$\mathbf{n}^\eta(\eta) = \frac{1}{\left| \begin{Bmatrix} -y(\eta) \\ x(\eta) \end{Bmatrix} \right|} \begin{bmatrix} -y(\eta) & 0 \\ 0 & x(\eta) \\ x(\eta) & -y(\eta) \end{bmatrix} \quad (18)$$

For 1D sub-parametric elements of the DSBFEM, the mapping functions $\boldsymbol{\varphi}(\eta)$ are different from the shape functions $\mathbf{N}(\eta)$. For an element with $(n_\eta + 1)$ nodes, the proposed shape functions $N_i(\eta)$ of degree of $(2n_\eta + 1)$ are written as:

$$N_i(\eta) = \sum_{m=0}^{2n_\eta+1} a_m \eta^m \quad (19)$$

which have two special characteristics: (a) the shape functions have Kronecker Delta property, and (b) their first derivatives are equal to zero at any given node as:

$$N_{\alpha}(\eta_{\beta}) = \delta_{\alpha\beta} \tag{20}$$

$$N_{\alpha,\eta}(\eta_{\beta}) = 0 \tag{21}$$

For each element, the positions of nodes of shape and mapping functions are the same.

The displacement field $\mathbf{u}(\xi, \eta)$ at any point (ξ, η) is obtained by interpolation of the displacement function using the shape functions. In the proposed method, only domain's boundaries may be discretized. Therefore, the displacement field is written as:

$$\mathbf{u}(\xi, \eta) = N(\eta)\mathbf{u}(\xi) = N(\eta) \begin{Bmatrix} u_x(\xi) \\ u_y(\xi) \end{Bmatrix} \tag{22}$$

The strain vector at any point (ξ, η) may be derived using Eqs. (14, 15), and 22 as given by the following equation:

$$\boldsymbol{\varepsilon}(\xi, \eta) = \begin{Bmatrix} \varepsilon_{\hat{x}} \\ \varepsilon_{\hat{y}} \\ \gamma_{\hat{x}\hat{y}} \end{Bmatrix} = \mathbf{B}^1 \mathbf{u}_{,\xi}(\xi) + \frac{1}{\xi} \mathbf{B}^2 \mathbf{u} \tag{23}$$

in which

$$\mathbf{B}^1(\eta) = \mathbf{b}^1(\eta)N(\eta) \tag{24}$$

$$\mathbf{B}^2(\eta) = \mathbf{b}^2(\eta)N_{,\eta}(\eta) \tag{25}$$

Based on the Hook's law, the relation between strain and stress fields is written as:

$$\begin{aligned} \boldsymbol{\sigma}(\xi, \eta) &= \mathbf{D} \boldsymbol{\varepsilon}(\xi, \eta) \\ &= \mathbf{D} \left(\mathbf{b}^1 \mathbf{N} \mathbf{u}_{,\xi} + \frac{1}{\xi} \mathbf{b}^2 \mathbf{N} \right) \end{aligned} \tag{26}$$

where \mathbf{D} denotes the elasticity matrix of the problem.

The governing equilibrium equations for elastostatic problems may be illustrated as:

$$\sigma_{ij,j} + f_i = 0 \tag{27}$$

in which f_i indicates the body forces. For a 2D problem in domain Ω in global coordinates, $i = \hat{x}, \hat{y}$ and $j = \hat{x}, \hat{y}$. Instead of direct solving the strong form of Eq. (27), one may use a weak form by employing the weighted residual method. For this goal, Eq. (27) is weighted with an arbitrary weighting function (w), and integrated over the problem domain Ω . It may be shown that the SBFEM results in the following set of differential equations for elastostatic problems:

$$\xi \mathbf{D}^0 \mathbf{u}_{,\xi\xi}(\xi) + \mathbf{D}^1 \mathbf{u}_{,\xi}(\xi) + \xi \mathbf{F}(\xi) = \mathbf{0} \tag{28}$$

where

$$\mathbf{D}^0 = \int_{-1}^{+1} \mathbf{B}^{1T}(\eta) \mathbf{D} \mathbf{B}^1(\eta) |\mathbf{J}(\eta)| d\eta \tag{29}$$

$$\mathbf{D}^1 = \int_{-1}^{+1} \mathbf{B}_{,\eta}^{1T}(\eta) \mathbf{D} \mathbf{B}^2(\eta) |\mathbf{J}(\eta)| d\eta \tag{30}$$

$$\mathbf{F}(\xi) = \int_{-1}^{+1} \mathbf{N}^T(\eta) \mathbf{f}(\xi, \eta) |\mathbf{J}(\eta)| d\eta \tag{31}$$

in which $\mathbf{F}(\xi) = \{F_{\hat{x}}(\xi), F_{\hat{y}}(\xi)\}^T$ indicates the nodal vector of the body forces.

To calculate the coefficient matrices $\mathbf{D}^0, \mathbf{D}^1$, and the vector $\mathbf{F}(\xi)$, the Clenshaw–Curtis quadrature rule for 2D analyses at the CLL points is used in DSBFEM. Employing the Clenshaw–Curtis quadrature as well as special shape functions leads to diagonal coefficient matrices. Therefore, the set of differential equations (Eq. (28)) may be expressed as a set of decoupled differential equations regarding a specific node i as:

$$\xi D_{ii}^0 u_{i,\xi\xi}(\xi) + D_{ii}^1 u_{i,\xi}(\xi) + \xi F_i(\xi) = 0 \tag{32}$$

It should be noted that Eq. (32) refers to an Euler's differential equation that depends only on the elastostatic function of the i th degrees of freedom (DOF). This means that the coupled set of differential equations has been transferred to decoupled differential equations using special mapping functions, shape functions, and quadrature, through the weighted residual method.

3. Modification of the DSBFEM

Else the mapping functions, control points and the numerical integration technique, the modeling and solution procedure used in the present work is similar to that study which is published in [41]. Here in, against of the previous DSBFEM, a set of higher-order Lagrange polynomials are used in order to interpolation of the model, and geometry, where these mapping functions are set up on GLL points as control points and employing the Gauss-Lobatto-Legendre quadrature for calculating the matrices, leads to decoupled partial differentials.

3.1. Lagrange polynomials as mapping function

For a $(n_\eta + 1)$ node element, a Lagrange polynomial of n_η is used; these polynomials for the i th point will be calculated as:

$$\varphi_i(\eta) = \prod_{k=1, k \neq i}^{n_\eta+1} \frac{\eta - \eta_k}{\eta_i - \eta_k} \quad (33)$$

Considering Eq. (33), the Lagrange polynomials have the properties of the Kronecker Delta at any control point as:

$$\varphi_\alpha(\eta_\beta) = \delta_{\alpha\beta} \quad (34)$$

As it is clear for preparing an order n_η parent element, $(n_\eta + 1)$ nodes are required where two end-nodes are located at the extremity ($\eta = \pm 1$) of the element and other $(n_\eta - 1)$ remained internal nodes are located at the Gauss-Lobatto-Legendre points, which are the roots of the first-order derivative of order n_η Legendre polynomial [39]:

$$\frac{d}{d\eta} P_{n_\eta}(\eta) = 0 \quad (35)$$

where, the Legendre polynomial of order n_η is expressed using Rodrigues' formula as:

$$P_{n_\eta}(\eta) = \frac{1}{2^n n!} \frac{d^{n_\eta}}{d\eta^{n_\eta}} \left[(\eta^2 - 1)^{n_\eta} \right] \quad (36)$$

in which $i = 0, 1, 2, \dots, (n_\eta + 1)$

3.2. Gauss-Lobatto-Legendre quadrature

In this study, to calculate the vectors and matrices in Eq. (28), the Gauss-Lobatto-Legendre numerical integration method is applied to calculate the values of the coefficients matrix in the GLL. According to the node element that corresponds to the points and also features a shape functions used, resulting diagonal matrix of coefficients used in the equation. Weight coefficients used in the method of integration is calculated using the following equation:

$$W_i = \frac{2}{n_\eta(n_\eta + 1) \left(P_{n_\eta}'(\eta_i) \right)^2} \quad (37)$$

Consequently, the components of coefficient matrices may be expressed as:

$$D_{ij}^0 = 2\delta_{ij} W_i \mathbf{B}^{1T}(\eta_i) \mathbf{D} \mathbf{B}^1(\eta_i) | \mathbf{J}(\eta_i) | \quad (38)$$

$$D_{ij}^1 = 2\delta_{ij} W_i \mathbf{B}_{,\eta}^{1T}(\eta_i) \mathbf{D} \mathbf{B}^2(\eta_i) | \mathbf{J}(\eta_i) | \quad (39)$$

where δ_{ij} denotes the Kronecker Delta which results in diagonal coefficient matrices. So, the system of partial differential Eq. (28) may be expressed as a single differential equation regarding to a specified point i as the following expression:

$$\xi D_{ii}^0 u_{i,\xi\xi}(\xi) + D_{ii}^1 u_{i,\xi}(\xi) + \xi F_i(\xi) = 0 \quad (40)$$

It is worthwhile remarking that Eq. (40) offers a set of ordinary differential equations for an elastostatic problem with $2n$ DOFs. Each differential equation in Eq. (40) depends only on the elastostatic function of the i th DOF. This

means that the coupled system of differential equations has been transformed into decoupled differential equations using a special set of weak formulation procedure, mapping functions, quadrature, and shape functions. In other words, to evaluate the displacement function and its derivatives at a given point, the governing equation that is corresponding to the point should be solved, only. As may be illustrated later, the decoupled differential equations system proposed in this study can also provide higher rates of convergence by employing a few numbers of DOFs compared to other numerical methods.

4. The DSBFEM in cracked media

Based on Sections 2 and 3, in order to use this method in fracture mechanics problems, the geometrical and physical modeling is discussed. Therefore, the procedure of implementing fracture mechanics issues in DSBFEM is explained in the following two sub-sections [40].

4.1. Geometrical modeling

To model the cracked domains in the present method, the geometry of cracks is modeled in very small void spaces, at the first step. According to fracture mechanics relationships, it is necessary to rewrite governing equations in polar coordinates, in the proposed semi-analytical method. Fig. 2 depicts a cracked domain modeled by the DSBFEM, in which the LCO is placed at the crack tip. Therefore, a simple relationship between (ξ, η) and (r, θ) coordinates, with the LCO at the crack tip, may be written as:

$$r^2 = \hat{x}^2 + \hat{y}^2 \tag{41}$$

and

$$\theta = \tan^{-1}\left(\frac{\hat{y}}{\hat{x}}\right) = \tan^{-1}\left(\frac{y(\eta)}{x(\eta)}\right) \tag{42}$$

By substituting Eqs. (6 and 7) into Eq. (41), one can write

$$r = \xi r_\eta(\eta) \tag{43}$$

where

$$r_\eta(\eta) = \sqrt{x^2(\eta) + y^2(\eta)} \tag{44}$$

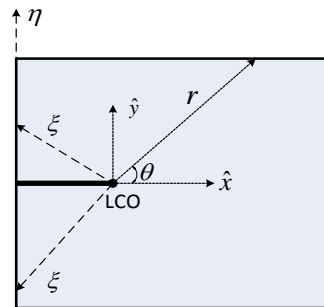


Fig. 2. A 2D cracked domain modeled by the DSBFEM.

4.2. Physical modeling

One of the other important stages of crack modeling in the DSBFEM is to implement the crack conditions in the solution procedure, to consider infinite stress at the crack tip. As may be observed from Eq. (40), the order of displacement function $u_i(\xi)$ depends on $F_i(\xi)$.

In elastostatic problems, $F_i(\xi)$ varies in the undertaken domain like a body force. Therefore, $F_i(\xi)$ is defined as a linear function such as $a_i \xi + b_i$, in which a_i and b_i are obtained according to traction conditions in the LCO and at the boundaries [38]. The proposed form of force function basically provides inappropriate displacement functions $u_i(\xi)$ for crack problems, as is not capable to produce infinite stresses at the crack tip. It is thus necessary to change the form of displacement function in this regard. Therefore, in fracture mechanics issues, a new form of force function is proposed to consider crack conditions of infinite stress at the crack tip, as given by:

$$F(\xi) = \frac{a}{\sqrt{\xi}} + \frac{b}{\xi \sqrt{\xi}} \tag{45}$$

by which the stress approaches infinity at the crack tip, when $\xi \rightarrow 0$. Therefore, Eq. (40) may be rewritten as the following relation:

$$\xi D_{ii}^0 u_{i,\xi\xi} + D_{ii}^1 u_{i,\xi} + \xi \left(\frac{a_i}{\sqrt{\xi}} + \frac{b_i}{\xi\sqrt{\xi}} \right) = 0 \tag{46}$$

It may be shown that the general solution of the above differential equation for the *i*th DOF, may be given as:

$$u_i(\xi) = A_i \xi^{\left(\frac{D_{ii}^0 - D_{ii}^1}{D_{ii}^0} \right)} + \frac{B_i}{(D_{ii}^0 - D_{ii}^1)} - \frac{4a_i}{(D_{ii}^0 - 2D_{ii}^1)} \sqrt{\xi} - \frac{4b_i}{3(D_{ii}^0 + 2D_{ii}^1)} \xi \sqrt{\xi} \tag{47}$$

where A_i and B_i denote the constant coefficients which are evaluated by imposing the BCs at $\xi=0,1$, corresponding to the *i*th DOF. The BCs for the DOFs of the domain's boundary are those of Dirichlet (\bar{u}_i) or Neumann (\bar{T}_i) ones, in which \bar{u}_i and \bar{T}_i denote the known values of displacements and tractions, respectively (see Fig. 3).

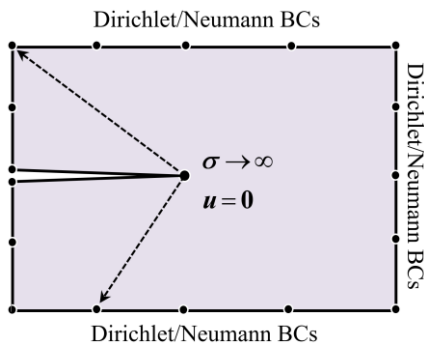


Fig. 3. Various Dirichlet or Neumann BCs for the crack tip and domain's boundary DOFs.

5. Solution procedure

As discussed before, the coefficient matrices have become diagonal as a set of single Euler's

differential equations for the *i*th DOF. If n implies the number of DOFs of the problem supposed to be solved by the DSBFEM, only n Euler's differential equations (with only one unknown differential equation for each DOF) should be solved. In other words, the DSBFEM offers an efficient procedure for solving various problems as already reported in Refs. [37-42]. In this section, the required procedure for solving Euler's differential equations fracture mechanics problems is explained. The solution procedure of the DSBFEM based on the novel modifications in the fracture mechanics is summarized in the following steps:

- The coefficient matrices for all DOFs are determined at the first step, along \hat{x} and \hat{y} directions, separately.
- Implementing the boundary conditions (BCs) of the problem, the governing differential equations are then solved for the DOFs excited by the external forces. Therefore, the displacement field of the problem's domain along radial coordinate ξ , related to the *i*th DOF is obtained in this step.
- At the third step, the stress components along radial coordinate ξ corresponding to the *i*th DOF is obtained using Eq. (26).
- Finally, using the equilibrium equation, the internal stress components at the LCO, σ_{LCOi} , are determined for each DOF.

In the DSBFEM, the LCO is identical for all nodes, for which the LCO has the same displacement components. Consequently, the physical concept of this fact may be considered as parallel springs adjoining to each other at the LCO (see Fig. 4). To calculate the inner stresses at the LCO, the inner stress from each DOF is summed up at the LCO as given by:

$$\sigma_{LCO} = \sum_{i=1}^n \sigma_{LCOi} \tag{48}$$

In this regard, the contribution of each DOF for the inner stresses of Eq. (48) may be computed by:

$$\sigma_{LCOi} = \frac{D_{ii}^0}{\sum_{j=1}^n D_{jj}^0} \sigma_{LCO} \quad (49)$$

The governing Euler's differential equations with the internal body forces are then solved. For each DOF, the internal body forces may be obtained from internal stresses at the LCO, as a body force along ξ (see Eq. (40)) as given by:

$$f_i(\xi) = \mathbf{n}^{\eta T}(\eta) \sigma_i(\xi) \quad (50)$$

It should be noted that the proposed procedure of this section is similar to the moment distribution procedure of classic structural analysis. Therefore, the proposed procedure is called "redistribution" in the DSBFEM.

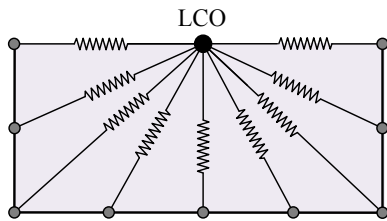


Fig. 4. The physical concept of the solution procedure of the problem.

At the final step, using the calculated displacement field along ξ , the displacement at any point of the problem's domain may be interpolated by employing the proposed special shape functions. Although in the present method, the governing equation of each DOF is decoupled from those of other DOFs, however, the "redistribution" of the stresses at the LCO and resolving the problem for each DOF, represents the connection between all DOFs of the problem.

6. Calculation of SIFs

Williams showed that the stress and displacement in cracked media are expressed by infinite series [1]. The analysis of cracked domains based on the LEFM shows an infinite stress state at the crack tip, in which no material can resist such an infinite stress state. Therefore, instead of comparing the infinite

stress field with a strength criterion, fracture mechanics adopts the SIFs or the first order terms of Williams's series to illustrate existing singular stress field in the vicinity of the crack tip. In addition, the SIFs are the most important parameters for predicting crack propagation [2]. Recently, Berto and Lazzarin have shown that the T-stress or the second order terms of Williams's series are important to show the stress field in the crack tips [44].

There are various analytical and numerical methods to compute the SIFs in the literature, such as using displacement or stress field [29], J-integral method (based on the theorem of energy conservation) [45, 46], and energy release rate technique (according to elastic strain energy release respect to crack growth) [47]. Each of these methods has its own advantages. For example, in using displacement or stress field, the SIFs may be calculated directly, while in energy release rate technique, the SIFs may be evaluated with coarse meshes. In this study, displacement field (as a direct method) and energy release rate technique (as an indirect method) is employed to evaluate the fractures' parameters at the crack tip.

The SIFs of mode-I and mode-II by using of displacement field are computed by using the following relations [2]:

$$K_I = \lim_{r \rightarrow 0} \left(\frac{2\mu}{\kappa + 1} \sqrt{\frac{2\pi}{r}} u_y \Big|_{\theta=0} \right) \quad (51)$$

$$K_{II} = \lim_{r \rightarrow 0} \left(\frac{2\mu}{\kappa + 1} \sqrt{\frac{2\pi}{r}} u_x \Big|_{\theta=0} \right) \quad (52)$$

in which μ denotes the elastic shear modulus. Furthermore, $\kappa = \frac{3-\nu}{1+\nu}$ for plane stress condition, while $\kappa = 3 - 4\nu$ for plane strain one, in which ν indicates Poisson's ratio. The advantage of the direct method is that the SIFs may be usually obtained directly without further processing and computational efforts. The main disadvantage of the direct method may be devoted to the fine mesh requirements as well as singularities around the crack tip. Therefore,

in the DSBFEM Eqs. (51 and 52) can be rewritten as:

$$K_I = \lim_{\xi \rightarrow 0} \left(\frac{2\mu}{\kappa+1} \sqrt{\frac{2\pi}{r(\eta)\xi}} u_y(\xi) \Big|_{\eta=-1} \right) \quad (53)$$

$$K_{II} = \lim_{\xi \rightarrow 0} \left(\frac{2\mu}{\kappa+1} \sqrt{\frac{2\pi}{r(\eta)\xi}} u_x(\xi) \Big|_{\eta=-1} \right) \quad (54)$$

Also, the energy release rate method as an indirect procedure is used in this study to evaluate the fracture parameters. The advantage of the energy release rate method is that the crack tip stress field, which is singular and corresponds to an unreal situation in practice, makes only a relatively small contribution to the total strain energy of the cracked media. Significant applications of energy release method are in crack propagation and failure analysis. Let's consider the energy release rate. The energy release rate G is defined as:

$$G = - \frac{d\Pi}{da} \quad (55)$$

in which a is the length of the crack, and Π denotes the elastic strain energy in Ω domain as given by:

$$\Pi = \int_{\Omega} W d\Omega = \frac{1}{2} \int_{\Omega} \boldsymbol{\sigma}^T \boldsymbol{\varepsilon} d\Omega \quad (56)$$

where W is the strain energy density. G may be calculated from the rate of modification in the elastic strain energy Π with respect to a crack growth Δa . In practice applications, G is evaluated considering the variation of the global potential energy $\Delta\Pi$, when the crack growth is Δa , as written by the following relation:

$$G = - \frac{\Delta\Pi}{\Delta a} = - \frac{\Pi_2 - \Pi_1}{a_2 - a_1} \quad (57)$$

where Π_1 and Π_2 denote the elastic strain energies related to the crack lengths of a_1 and a_2 , respectively. Finally, to calculate the

SIFs, the relations of energy release rate G and the SIFs for mixed modes I and II are:

$$G_I = \frac{\kappa+1}{8\mu} (K_I^2 + K_{II}^2) \quad (58)$$

$$G_{II} = \frac{\kappa+1}{8\mu} (-2K_I K_{II}) \quad (59)$$

In the energy release rate approach, to compute the SIFs (see Eq. (57)), the total elastic strain energy of the cracked media is calculated. So, the elastic strain energy Π^e for any sub-domain Ω^e is defined as (see Fig. 5):

$$\Pi^e(\xi, \eta) = \frac{1}{2} \int_{\Omega^e} \boldsymbol{\sigma}^T(\xi, \eta) \boldsymbol{\varepsilon}(\xi, \eta) d\Omega^e \quad (60)$$

or

$$\begin{aligned} \Pi^e(\xi, \eta) &= \frac{1}{2} \int_{-1}^{+1} \int_{-1}^{+1} \boldsymbol{\sigma}^T(\xi, \eta) \boldsymbol{\varepsilon}(\xi, \eta) \xi |J| d\eta d\xi \quad (61) \end{aligned}$$

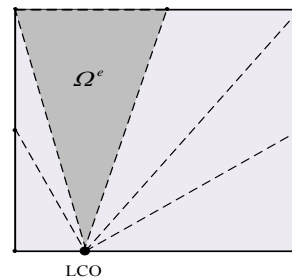


Fig. 5. Elastic strain energy for a sub-domain in the DSBFEM.

Based on Eqs. (23 and 26), the stress and strain fields are determined analytically in the radial direction ξ , and therefore, the integrated form of Eq. (61) is solved analytically in the radial direction. In the tangential direction η , Eq. (61) is solved numerically using the Gauss-Lobatto-Legendre quadrature at GLL point. The total elastic strain energy is then computed by adding the strain energy of each sub-domain as:

$$\Pi = \sum_{i=1}^{n_e} \Pi_i^e \quad (62)$$

where n_e denotes the number of elements. Finally, based on Eq. (57) the released energy rate is computed according to a very small virtual growth of crack length, in the following numerical examples.

7. Numerical examples

The accuracy and efficiency of the present method for analysis of crack problems, based on direct and indirect method, is illustrated through three 2D benchmark problems. The results determined from the present approach are compared with other existing numerical methods available in the literature.

7.1. Cracked plate under uniaxial tension

The first example studies a through-thickness cracked plate. The plate contains a central crack and is subjected to tensile stress with intensities of $\sigma = 1$ units applied on both sides of the plate (see Fig. 6). In this example, the plane stress status is considered, for which the elastic modulus and Poisson's ratio are $E = 1$ unit and $\nu = 0.3$, respectively.

Due to the symmetrical condition of the problem, only one-quarter of the plate is modeled as shown in Fig. 7(a). As Fig. 7(b) shows, the boundaries of the domain are divided into 15 three-node elements with total 62 DOFs. This example represents a pure mode-I problem.

In order to assess the accuracy of the first example, the experimental results are used [48] for comparison. To calculate the SIF of mode-I, one may write:

$$K_I = F\sigma\sqrt{\pi a} \tag{60}$$

in which

$$F = 1 + 0.13\left(\frac{a}{b}\right) - 0.29\left(\frac{a}{b}\right)^2 + 15.25\left(\frac{a}{b}\right)^3 \tag{61}$$

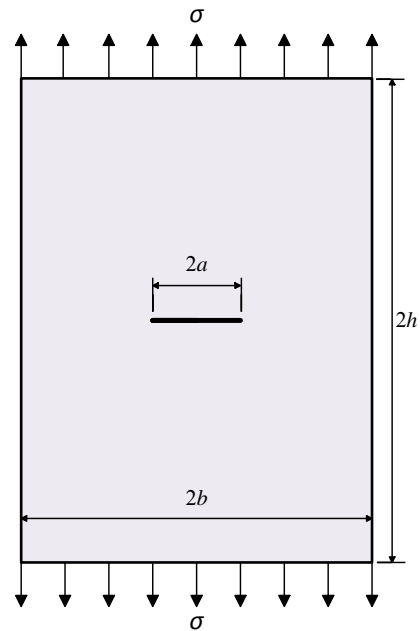


Fig. 6. The BCs and geometry of the first numerical example.

Using the energy release rate approach, the first numerical example problem is solved, whose SIF results are shown in Table 1, for various differential crack lengths (Δa). To get better sense on the obtained results, the errors of the proposed method compared to the experimental results [48] are demonstrated in Fig. 8. Obviously, the results of the present method agree very well with available experimental results. Figure 8 shows that very small values Δa (say $\Delta a = 0.0001$) yields to converged results to real experimental values.

Table 1. Determination of the SIF and the rate of SIF for mode-I in the cracked plate of the first example.

| Δa | Present study | | DSBFEM | |
|------------|---------------|-----------------------------------|--------|-----------------------------------|
| | K_I | $\frac{\partial K_I}{\partial a}$ | K_I | $\frac{\partial K_I}{\partial a}$ |
| 0.01 | 2.861 | 0.735 | 2.837 | 0.738 |
| 0.005 | 2.871 | 0.740 | 2.850 | 0.742 |
| 0.001 | 2.879 | 0.744 | 2.864 | 0.746 |
| 0.0002 | 2.928 | 0.745 | 2.916 | 0.747 |
| 0.0001 | 3.010 | 0.745 | 3.000 | 0.747 |

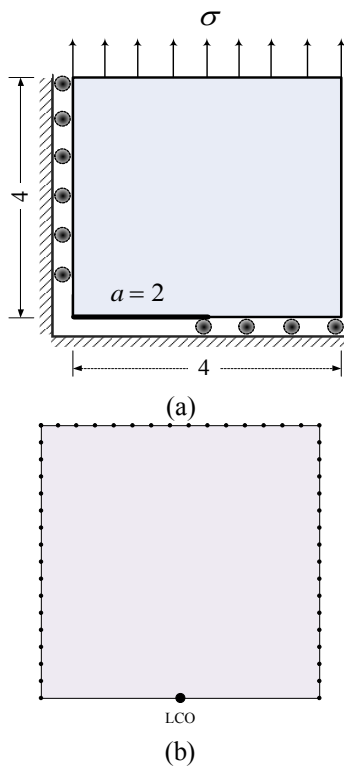


Fig. 7. (a) The BCs and geometry considered for one quarter of the first example plate, and (b) the mesh used for modeling of the example, in which the LCO and nodes of elements are depicted.

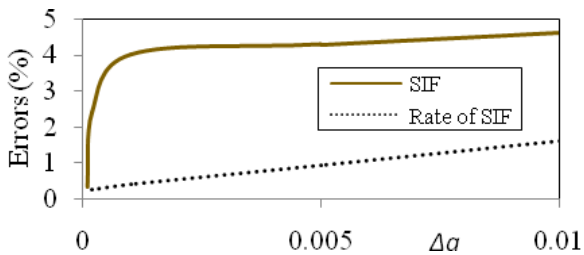


Fig. 8. The errors of K_I and $\partial K_I/\partial a$ of the present study for the first example.

Furthermore, due to independence of $\partial K_I/\partial a$ to a , it represents minimal errors. In addition, Fig. 9(a) shows the stress distribution of the crack tip as well as the whole cracked domain. Also, the accuracy of the stress distribution is evaluated in Fig. 9(b), in which the results of the present method are compared with those of Ref. [12].

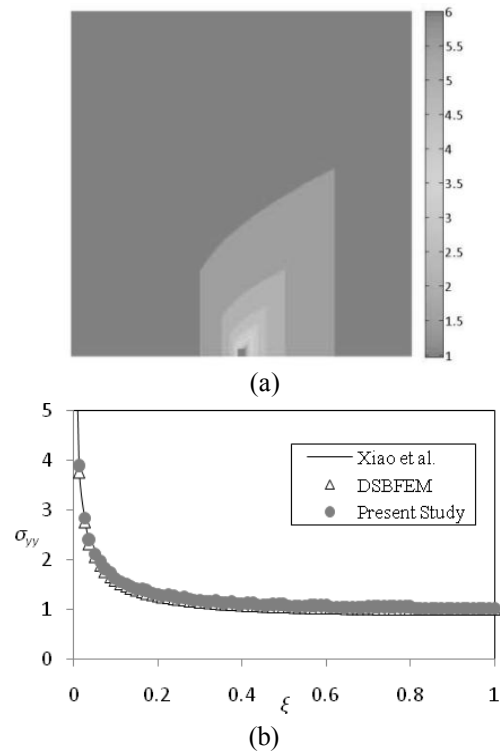


Fig. 9. The stress distribution (σ_{yy}) for (a) the whole cracked domain and (b) along the crack tip in the direction of loading ($\sigma=1, a=2$), for the first example.

7.2. Edge-cracked plate under shear traction

The second example examines an edge-cracked plate, which is constrained at the end, and is loaded by shear stress $\tau = 1$ unit applied on the top of the plate. The geometry and BCs are demonstrated in Fig. 10. This problem may be considered as an example of a Mixed-Mode problem. The elastic modulus and Poisson's ratio are $E = 30 \times 10^6$ unit and $\nu = 0.25$, respectively. The mesh is similar to that of Fig. 7(b), whose boundary is divided into 46 three-node elements with total 186 DOFs used. Again, the problem is solved based on displacement field approach as an indirect method and the results of the present method are compared to two other available results [40, 49], as shown in Tables 2 and 3. The tables imply very good agreement with the referenced results, for which the maximum error is less than 5 percent.

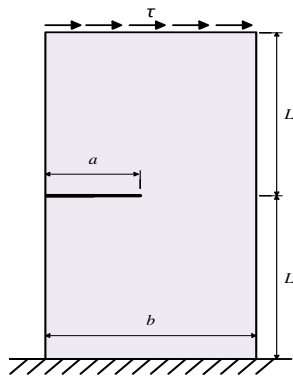


Fig. 10. The geometry and BCs of the second numerical example.

Table 2. Determination of the SIFs for mode-I in the edge-cracked plate of the second numerical example.

| a/b | DSBFEM | SBFEM | The present study | Error (%) |
|-------|--------|-------|-------------------|-----------|
| 0.3 | 19.56 | 19.80 | 19.54 | 0.70 |
| 0.4 | 25.73 | 25.64 | 25.69 | 0.17 |
| 0.5 | 34.24 | 34.04 | 34.18 | 0.29 |

Table 3. Determination of the SIFs for mode-II in the edge-cracked plate of the second numerical example.

| a/b | DSBFEM | SBFEM | The present study | Error (%) |
|-------|--------|-------|-------------------|-----------|
| 0.3 | 2.52 | 2.46 | 2.54 | 2.02 |
| 0.4 | 3.62 | 3.49 | 3.67 | 3.28 |
| 0.5 | 4.69 | 4.54 | 4.73 | 2.51 |

7.3. Slanting crack under uniaxial tension

The third example is corresponding to an oblique-cracked plate, which is subjected to the tensile stress of $\sigma = 1$ unit applied on both sides, as demonstrated in Fig. 11(a). Again, the plane stress condition is taken into account. Because of the axis-symmetrical condition of the problem, half of the plate is considered as depicted in Fig. 11(b). The geometrical parameters of this finite plate are as follow: $a = 0.1$, $L = b = 1$, and $\theta = 60^\circ$. In addition, the elastic modulus $E = 1$, and Poisson's ratio $\nu = 0.3$. As shown in Fig. 11(c), the domain of this example is discretized into three subdomains which include 62, 14, and 16 three-node elements (a total number of 370 DOFs). For this example which requires a mixed-mode analysis, the direction of virtual crack extension Δa is not determined, while computing of G in all directions is necessary.

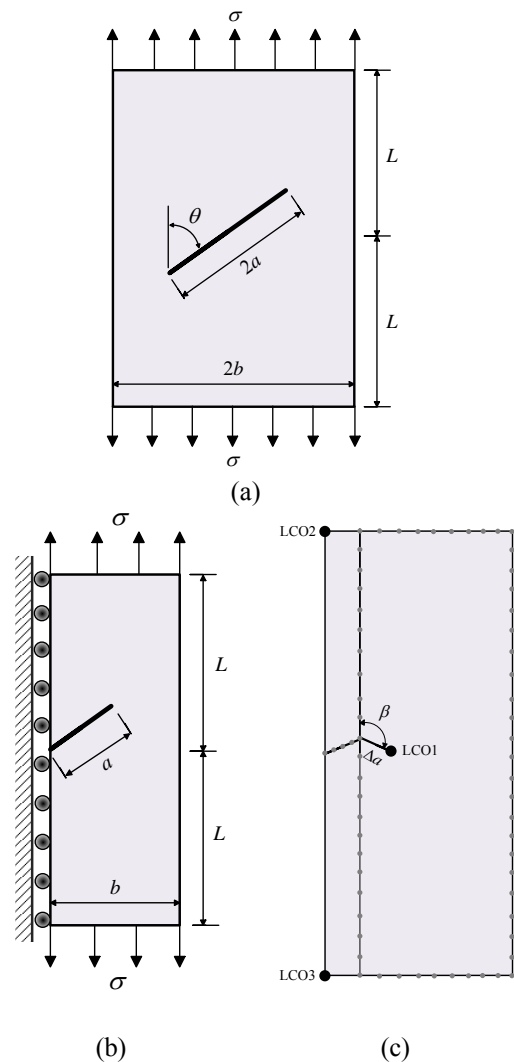


Fig. 11. The geometry and BCs considered for (a) the whole, (b) half of the plate, and (c) the mesh used for modeling of the third example using three LCOs.

Also using Eq. (57), various lengths of Δa are tried in evaluating G . Finally, the problem is solved, whose obtained results are compared with the results reported in Ref. [50], as demonstrated in Fig. 12. According to Fig. 12, the maximum value of G is corresponding to $\beta = 100^\circ$, which means that the direction of crack propagation is 40° clockwise from the direction of the crack axis. Again, the results of the present method show good agreement with the available results of Ref. [50].

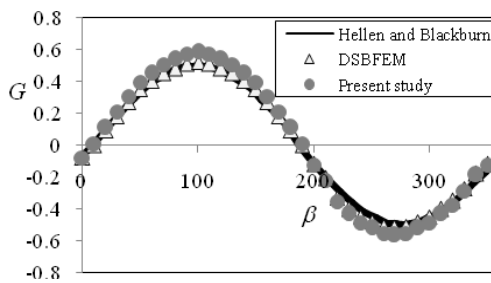


Fig. 12. Plot of G versus β with lengths of $\Delta a = 0.001$.

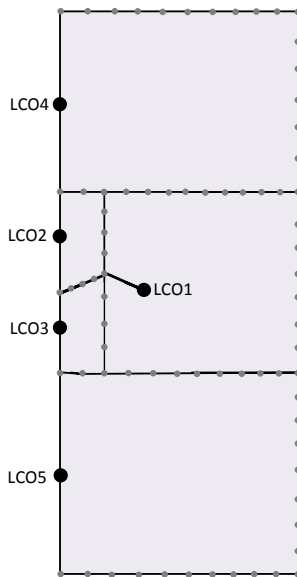


Fig. 13. The second mesh used for modeling of the third example using five LCOs.

In order to get a better sense of the accuracy of the present method's results, the convergence of the evaluated G is investigated. In addition to the Fig. 11(c), as shown in Fig. 13, the domain of this example is discretized into five subdomains which include 36, 10, 10, 32 and 32 three-node elements (a total number of 482 DOFs), and again the results display in the Fig. 14. Obviously, the results of the finest mesh of Fig. 14 shows the best accuracy. Consequently, the novel modification of the DSBFEM represents excellent converged results.

In the third numerical example for more consideration, some details are addressed. For instance, the CPU time required for computing G is 670 s (11 min and 10 s) in a standard PC equipped with a 3.1 GHz processor and 16 GB RAM in the previous DSBFEM. But

in the new version of DSBFEM, the time required for computing G is 582 s (9 min and 42 s) in a similar PC.

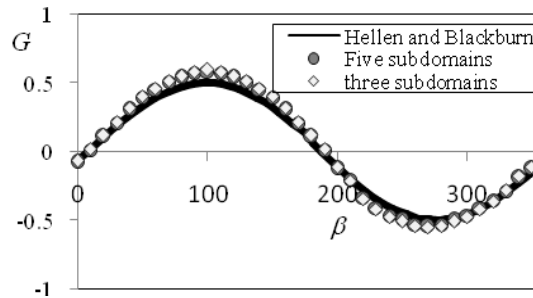


Fig. 14. Plot of G versus β with lengths of $\Delta a = 0.001$ for showing the divergence of the proposed technique in the third example.

8. Conclusions

In this research, a modification of the novel semi-analytical method, based on the scaled boundary finite element method that is called as DSBFEM, was studied. The procedure of the modeling and solution of the 2D fracture mechanics problems are similar to the DSBFEM. The difference in the proposed approach is that the boundary of the domain which was discretized by new higher-order sub-parametric elements with Lagrange polynomials as mapping functions, and the control points which were Gauss-Lobatto-Legendre points, and also, using Gauss-Lobatto-Legendre quadrature the coefficient matrices of equations system became diagonal. This led to a system of decoupled governing equations for the entire system. Some examples were successfully analyzed using the newly proposed technique. In these examples, various crack problems and various loading types were selected to display the generality and applicability of the present approach in the fracture mechanics issues. It should be mentioned that all the examples were successfully modeled with a very small number of DOFs and less complexity, preserving very high accuracy compared to the available analytical and numerical solutions. By implementing the novel modifications, the most remarkable advantage of the proposed method again DSBFEM was its low totally computational efforts.

Acknowledgements

The author would like to acknowledge and express their special gratitude to Prof. N. Khaji and Dr. M. I. Khodakarami, for their constructive remarks that improved the quality of the manuscript.

References

- [1] M. L. Williams, "On the stress distribution at the base of a stationary crack", *Journal of Applied Mechanics*, Vol. 24, No. 1, pp. 109-114, (1957).
- [2] D. Broek, *Elementary engineering fracture mechanics*, Springer, (1986).
- [3] S. Aoki, K. Kishimoto, H. Kondo, M. Sakata, "Elastodynamic analysis of crack by finite element method using singular element", *International Journal of Fracture*, Vol. 14, No. 1, pp. 59-68, (1978).
- [4] M. R. Ayatollahi, M. Nejati, "An over-deterministic method for calculation of coefficients of crack tip asymptotic field from finite element analysis", *Fatigue and Fracture of Engineering Materials and Structures*, Vol. 34, No. 3, pp. 159-176, (2011).
- [5] M. Bäker, "Finite element crack propagation calculation using trial cracks", *Computational Materials Science*, Vol. 43, No. 1, pp. 179-183, (2008).
- [6] E. P. Chen, "Finite element analysis of a bimaterial interface crack", *Theoretical and Applied Fracture Mechanics*, Vol. 3, No. 3, pp. 257-262, (1985).
- [7] H. G. Delorenzi, "Energy release rate calculations by the finite element method", *Engineering Fracture Mechanics*, Vol. 21, No. 1, pp. 129-143, (1985).
- [8] R. D. Henshell, K.G. Shaw, "Crack tip finite elements are unnecessary", *International Journal for Numerical Methods in Engineering*, Vol. 9, No. 3, pp. 495-507, (1975).
- [9] S. Mohammadi, *Extended finite element method: for fracture analysis of structures*, John Wiley & Sons, (2008).
- [10] K. Sharma, T.Q. Bui, C. Zhang, R.R. Bhargava, "Analysis of a subinterface crack in piezoelectric bimaterials with the extended finite element method", *Engineering Fracture Mechanics*, Vol. 104, pp. 114-139, (2013).
- [11] H. Pathak, A. Singh, I.V. Singh, S.K. Yadav, "Fatigue crack growth simulations of 3-D linear elastic cracks under thermal load by XFEM", *Frontiers of Structural and Civil Engineering*, Vol. 9, No. 4, pp. 359-382, (2015).
- [12] Q. Z. Xiao, B. L. Karihaloo, "Improving the accuracy of XFEM crack tip fields using higher order quadrature and statically admissible stress recovery", *International Journal for Numerical Methods in Engineering*, Vol. 66, No. 9, pp. 1378-1410, (2006).
- [13] A. Portela, M. H. Aliabadi, D. P. Rooke, "Efficient boundary element analysis of sharp notched plates", *International Journal for Numerical Methods in Engineering*, Vol. 32, No. 3, pp. 445-470, (1991).
- [14] A. Portela, M. H. Aliabadi, D. P. Rooke, "Dual boundary element incremental analysis of crack propagation", *Computers & Structures*, Vol. 46, No. 2, pp. 237-247, (1993).
- [15] A. L. Saleh, M. H. Aliabadi, "Crack growth analysis in concrete using boundary element method", *Engineering Fracture Mechanics*, Vol. 51, No. 4, pp. 533-545, (1995).
- [16] A. Ghorbanpoor, J. Zhang, "Boundary element analysis of crack growth for mixed-mode center slant crack problems", *Engineering Fracture Mechanics*, Vol. 36, No. 5, pp. 661-668, (1995).
- [17] E. D. Leonel, W. S. Venturini, A. Chateaufneuf, "A BEM model applied to failure analysis of multi-fractured structures", *Engineering Failure Analysis*, Vol. 18, No. 6, pp. 1538-1549, (2011).

- [18] M. Treifi, S. O. Oyadiji, "Strain energy approach to compute stress intensity factors for isotropic homogeneous and bi-material V-notches", *International Journal of Solids and Structures*, Vol. 50, No. 14-15, pp. 2196-2212, (2013).
- [19] G. Meneghetti, B. Atzori, A. Campagnolo, F. Berto, "A link between the peak stresses and the averaged strain energy density for cracks under mixed-mode (I+II) loading", *Frattura ed Integrità Strutturale*, Vol. 9, No. 34, pp. 109-115, (2015).
- [20] N. O. Larrosa, M. Treifi, R.A. Ainsworth, "Rapid parametric analysis of SEN(T) specimens using algorithmic modelling: Evaluation of strain energy density and notch stress intensity factors", *Materials and Design*, Vol. 85, pp. 771-777, (2015).
- [21] P. Liu, T. Yu, T.Q. Bui, C. Zhang, "Transient dynamic crack analysis in non-homogeneous functionally graded piezoelectric materials by the X-FEM", *Computational Materials Science*, Vol. 69, pp. 542-558, (2013).
- [22] D. Racz, T.Q. Bui, "Novel adaptive meshfree integration techniques in meshless methods", *International Journal for Numerical Methods in Engineering*, Vol. 90, No. 11, pp. 1414-1434, (2012).
- [23] B. N. Rao, S. Rahman, "Probabilistic fracture mechanics by Galerkin meshless methods - Part I: Rates of stress intensity factors", *Computational Mechanics*, Vol. 28, 351-364, (2002).
- [24] N. T. Nguyen, T.Q. Bui, C. Zhang, T.T. Truong, "Crack growth modeling in elastic solids by the extended meshfree Galerkin radial point interpolation method", *Engineering Analysis with Boundary Elements*, Vol. 44, pp. 87-97, (2014).
- [25] S. Rajagopal, N. Gupta, "Meshfree modelling of fracture-a comparative study of different methods, *Meccanica*", Vol. 46, No. 5, pp. 1145-1158, (2011).
- [26] A. Asadpour, "Thermo-elastic extended meshfree method for fracture without crack tip enrichment", *Frontiers of Structural and Civil Engineering*, Vol. 9, No. 6, pp. 441-447, (2015).
- [27] A. Y. T. Leung, R. K. L. Su, "Mode I crack problems by fractal two level finite element methods", *Engineering Fracture Mechanics*, Vol. 48, 847-856, (1994).
- [28] J. Y. Liu, F. L. Xu, B. K. Ning, H. Fan, "Evaluation of the T-stress and the higher order terms of the elastic crack based on the SBFEM", *Advanced Materials Research*, Vol. 838, pp. 2275-2278, (2014).
- [29] C. Song, J. P. "Wolf, Semi-analytical representation of stress singularities as occurring in cracks in anisotropic multi-materials with the scaled boundary finite-element method", *Computers and Structures*, Vol. 80, No. 2, pp. 183-197, (2002).
- [30] S. R. Chidgze, A. J. Deeks, "Determination of coefficients of crack tip asymptotic fields using the scaled boundary finite element method", *Engineering Fracture Mechanics*, Vol. 72, No. 13, pp. 2019-2036, (2005).
- [31] Z. J. Yang, E. T. Ooi, "Recent progress in modeling crack propagation using the scaled boundary finite element method", *International Journal of Computational Methods*, Vol. 9, No. 1, pp. 1-24, (2012).
- [32] M. G. Shi, C. M. Song, H. Zhong, Y. J. Xu, C. H. Zhang, "A coupled SBFEM-FEM approach for evaluating stress intensity factors", *Applied Mechanics and Materials*, Vol. 353, pp. 3369-3377, (2013).
- [33] G. E. Bird, J. Trevelyan, C. E. Augarde, "A coupled BEM/scaled boundary FEM formulation for accurate computations in linear elastic fracture mechanics", *Engineering Analysis with Boundary Elements*, Vol. 34, No. 6, pp. 599-610, (2010).
- [34] B. N. Rao, S. Rahman, "A coupled meshless-finite element method for fracture analysis of cracks", *International Journal of Pressure Vessels and Piping*, Vol. 78, No. 9, pp. 647-657, (2001).

- [35] S. R. Chidgzey, J. Trevelyan, A. J. Deeks, "Coupling of the boundary element method and the scaled boundary finite element method for computations in fracture mechanics", *Computers and Structures*, Vol. 86, No. 11-12, 1198-1203, (2008).
- [36] Y. T. Gu, L. C. Zhang, "Coupling of the meshfree and finite element methods for determination of the crack tip fields", *Engineering Fracture Mechanics*, Vol. 75, No. 5, pp. 986-1004, (2008).
- [37] N. Khaji, M.I. Khodakarami, "A new semi-analytical method with diagonal coefficient matrices for potential problems", *Engineering Analysis with Boundary Elements*, Vol. 35, No. 6, 845-854, (2011).
- [38] M. I. Khodakarami, N. Khaji, "Analysis of elastostatic problems using a semi-analytical method with diagonal coefficient matrices", *Engineering Analysis with Boundary Elements*, Vol. 35, No. 12, pp. 1288-1296, (2011).
- [39] M. I. Khodakarami, N. Khaji, M. T. Ahmadi, "Modeling transient elastodynamic problems using a novel semi-analytical method yielding decoupled partial differential equations", *Computer Methods in Applied Mechanics and Engineering*, Vol. 213-216, No. 0, pp. 183-195, (2012).
- [40] N. Khaji, M. Yazdani, "Determination of stress intensity factors of 2D fracture mechanics problems through a new semi-analytical method", *Fatigue & Fracture of Engineering Materials & Structures*, Vol. 39, No. 4, pp. 467-478, (2016).
- [41] M. Yazdani, N. Khaji, M. Khodakarami, "Development of a new semi-analytical method in fracture mechanics problems based on the energy release rate", *Acta Mechanica*, Vol. 227, No. 12, pp. 3529-3547, (2016).
- [42] M. Yazdani, N. Khaji, M. Khodakarami, "Development of a new semi-analytical approach for 2D analysis of crack propagation problems", *Fatigue & Fracture of Engineering Materials & Structures*, 1-20, (2018).
- [43] M. I. Khodakarami, M. Fakharian, "A new modification in decoupled scaled boundary method with diagonal coefficient matrices for analysis of 2D elastostatic and transient elastodynamic problems", *Asian Journal of Civil Engineering*, Vol. 16, No. 5, pp. 709-732, (2015).
- [44] F. Berto, P. Lazzarin, "On higher order terms in the crack tip stress field", *International Journal of Fracture*, Vol. 161, No. 2, pp. 221-226, (2010).
- [45] J. R. Rice, "A Path Independent Integral and the Approximate Analysis of Strain Concentration by Notches and Cracks", *Journal of Applied Mechanics*, Vol. 35, No. 2, 379-386, (1968).
- [46] D. Nunez, K. S. Surana, A. Romkes, J. N. Reddy, "J-Integral for Mode I Linear Elastic Fracture Mechanics in h, p, k Mathematical and Computational Framework", *International Journal for Computational Methods in Engineering Science and Mechanics*, Vol. 10, No. 5, pp. 345-369, (2009).
- [47] H. G. deLorenzi, "On the energy release rate and the J-integral for 3-D crack configurations", *International Journal of Fracture*, Vol. 19, No. 3, pp. 183-193, (1982).
- [48] H. Tada, "Westergaard stress functions for several periodic crack problems", *Engineering Fracture Mechanics*, Vol. 2, No. 2, pp. 177-180, (1970).
- [49] M. S. Chowdhury, C. Song, W. Gao, "Probabilistic fracture mechanics by using Monte Carlo simulation and the scaled boundary finite element method", *Engineering Fracture Mechanics*, Vol. 78, No. 12, pp. 2369-2389, (2011).
- [50] T. K. Hellen, W. S. Blackburn, "The calculation of stress intensity factors for combined tensile and shear loading", *International Journal of Fracture*, Vol. 11, No. 4, pp. 605-617, (1975).

How to cite this paper:

M. Yazdani, “A novel modification of decouple scaled boundary finite element method in fracture mechanics problems”, *Journal of Computational and Applied Research in Mechanical Engineering*, Vol. 7. No. 2, pp. 243-260

DOI: 10.22061/jcarme.2017.1853.1161

URL: http://jcarme.srttu.edu/?_action=showPDF&article=766

